Cooling duct flow characterization using Particle Image Velocimetry and Laser Induced Fluorescence

Henrik Rochlitz
Research Assistant
TU Braunschweig – Institute of Fluid Mechanics
Hermann-Blenk-Straße 37, 38108 Braunschweig, Germany
H.Rochlitz@tu-bs.de

Peter Scholz
Head of Group Measurement and Manipulation of Flows
TU Braunschweig – Institute of Fluid Mechanics
Hermann-Blenk-Straße 37, 38108 Braunschweig, Germany
P.Scholz@tu-bs.de

ABSTRACT

This publication describes experimental investigations on a rectangular high-aspect ratio cooling duct flow with and without a heated wall under well-defined boundary conditions. The high-quality measurement techniques Particle Image Velocimetry and Laser Induced Fluorescence are utilized to identify and characterize the flow. The facility and the application of the measurement techniques are described. Detailed information about the flow including secondary flow structures and Reynolds stresses are given. A measurement of the temperature field is given. In addition, experimental results on the two color LIF technique with varying filters, concentrations and temperature are described.

1   INTRODUCTION

A detailed understanding of the flow and the heat transfer in cooling channels is important for designing optimal cooling circuits. This is particularly true for cooling channels with high heat loads and high thermal stresses, for example cooling circuits of rocket engines. Usually, the design process is based on RANS computations which often cannot be fully validated in detail due to missing experimental data. Therefore, the design margins must be high to prevent structural failure due to cyclic heat loads, e.g. the Dog House effect [1]. Hence, detailed measurements of the flow characteristics including local fluctuations of the temperature and the velocity field under well-defined conditions are necessary.

In most of the past experiments, merely integral values of the cooling ducts were taken from calorimetric analysis [2, 3, 4]. Rarely, measurements of time averaged flow fields in cooling ducts using gaseous fluids in large scale ducts were published [5]. Measurements of the velocity at discrete points using laser doppler velocimetry (LDV) systems were done more frequently. For example, Wardena et. al. [6, 7] applied LDV in a heated cooling duct with air.

Quantitative measurements of duct flow characteristics under well-defined boundary conditions including local fluctuations of the temperature and velocity fields are not available so far. However, these values can be measured using the high-quality, optical and non-invasive measurement techniques Particle Image Velocimetry (PIV) and Laser Induced Fluorescence (LIF). These experimental results can be used as a validation dataset for RANS and LES computations.

Hence, a cooling duct was designed, details are given in the following section. The flow fields in two and three dimensions is measured by the application of Particle Image Velocimetry (2C2D-PIV, i.e. two velocity

components in a plane), Stereo Particle Image Velocimetry (3C2D-PIV, i.e. three velocity components in a plane). A one color / one dye Laser Induced Fluorescence (1C-LIF) technique is used for first measurements of the temperature field in the duct flow. The duct flow is described in terms of the temperature and velocity fields. In the following section, improvements in the LIF technique, especially the application of a two color / two dye technique (2C-LIF) with different optical filters, is given. A detailed overview of improvements in the application of the LIF technique, especially in the application of a two color / two dye technique (2C-LIF) is given in the last section of this paper.

2   GENERIC COOLING DUCT SETUP

The experiments were performed in a high-aspect ratio generic cooling duct with water as the cooling fluid. An extensive parametric study resulted in the following geometry and design which is best suited for the desired experiment [8]. The cooling duct has a rectangular cross section with an average width of 6.2 mm and an average height of 26.1 mm (accordingly, the aspect ratio is 4.2).

The duct consists of a feed line with an identical cross section and a length of 600 mm, which is more than 60 times the hydraulic diameter. This feed line ensures a fully established turbulent duct flow at the beginning at the test section. The feed line is adiabatic, all walls and the fluid have the same temperature and no heat transfer occurs. The feed line is followed by the test section, which has a length of 600 mm, too. This length allows the formation of the thermal boundary layer. The test section's lower wall consists of copper and can be heated electrically. The lower wall is the tip of a so called heat nozzle: A massive copper block with a tapered tip. 23 cartridge heaters are embedded in the heat nozzle. The heat nozzle's tip temperature is measured at 23 positions along the duct using high precision resistance thermometers. A closed-loop system controls the cartridge heaters. Using this system, the duct's lower wall temperature is constant with a deviation less than 0.3 K of the desired temperature. The side and top walls are made of polymethyl methacrylate (PMMA) with a thickness of 10 mm to provide optical access to the flow. Possible optical distortions, caused by the PMMA walls, are corrected by means of a spatial calibration. The surface finish of all cooling duct walls was measured with a mechanical probe tip. The roughness average of all walls in the test section is of the same magnitude and all walls are hydraulically smooth. The surface roughness was measured before and after all measurements, no change in the roughness average values was observed.

An overview of the generic cooling duct setup is given in Figure 1 and Figure 2. The main flow direction is indicated by arrows. The coordinate system is shown in figure 1 as well. The point of origin is basically located in the center of the test section in y and z direction and 375 mm after the beginning of the test section in x direction. The system is a closed cycle and driven by a pump. The water flows from a tank through an electromagnetic flowmeter to the pump. An industrial rated flow straightener is mounted behind the pump, followed by a tube to the feed line. A second flow straightener is mounted just in front of the feed line to ensure a vortex free inflow. After passing the feed line and the test section, the water is routed back to the tank. The water temperatures and the absolute pressures are measured at the inlet of the feed line as well as at the outlet of the test section. The standard deviation divided by the mean value of the flow rate, measured with the electromagnetic flowmeter, is less than 0.6 %, which indicates that the fluctuations in the flow due to external disturbances are small. Heating devices with a heating output of 9 kW are installed in the tank to precondition the water to a desired bulk temperature
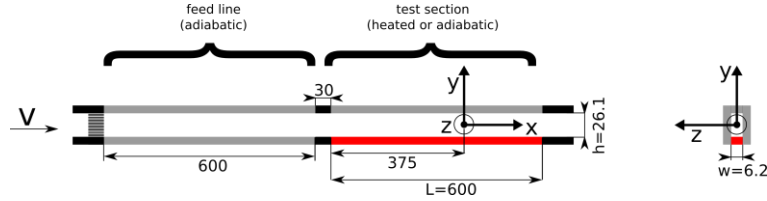
Figure 1: Dimensions of the high-aspect ratio cooling duct. The heated wall is indicated in red.
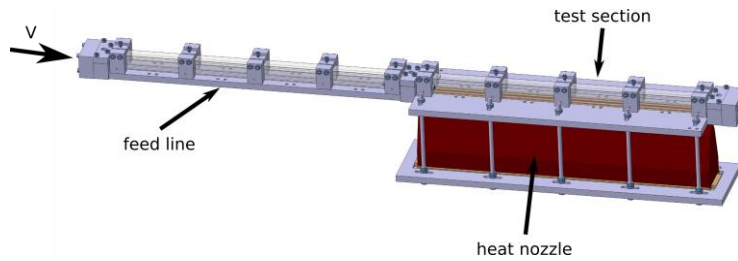

Figure 2: Overview of the generic cooling duct setup.

Furthermore, a cooling circuit allows cooling of the water with a maximum cooling power of 25 kW. These systems together ensure a constant and reliable inflow temperature within a range of ±0.2 K.
All velocity data in this publication is normalized by the bulk flow velocity which is defined as

$$u_b = \frac{\dot{V}}{A} \quad , \qquad (1)$$

with $\dot{V}$ being the flow rate and A the cross-sectional area of the duct. All turbulent values are normalized by u_b^2.

2.1   Configurations

The generic cooling duct allows different configurations regarding bulk and wall temperatures and flow rate resulting in a range of possible Reynolds numbers and heat fluxes. Herein, three different configurations were used. Table 1 gives an overview of the three cases. "Case 1" and "Case 2" are adiabatic cases with a change in Reynolds number by a change in bulk temperature. "Case 3" is basically "Case 2" with a heated wall respectively an applied heat flux.

| Case | $\dot{V}$ | T_b | T_w | $\dot{q}$ | Re |
	l/min	°C	°C	MW/m²	-
1	50	20	20	0	52000
2	50	60	60	0	111000
3	50	60	100	1.1	111000

Table 1: Parameters of the different flow cases

3   EXPERIMENTAL SETUP

PIV is an optical, non-invasive measurement techniques which is based on imaging of seeding particles in the flow, see [9] for detailed information. 2C2D-PIV and 3C2D-PIV techniques were used to measure the flow field in the generic cooling duct.

LIF is based on the fluorescence of special dyes being excited by incident light. A laser light is commonly used as the light source. The fluorescence intensity I is primarily based on the incident light flux I_0, the dye concentration C, an absorption coefficient ϵ, and the quantum efficiency ϕ:

$$I = I_0 C \epsilon \phi \ . \qquad (2)$$

All values except the quantum efficiency ϕ are temperature independent for most dyes, whereas the quantum efficiency ϕ is temperature dependent for special dyes. Rhodamine B has such physical characteristics and is used in all experiments described in this paper. Hence, the temperature of the dye respectively the dye dissolved in a liquid can be measured by measuring the fluorescence intensity. Using one dye is the so-called One-Color Laser Induced Fluorescence (1C-LIF).

Pulsed lasers have the disadvantage, that each individual laser pulse has a slightly different laser energy. Also, more-or-less stochastic variations of laser intensity across the field of view might occur. Hence, the incident light flux I_0 might vary over pulses or over the field, which increases effective uncertainty and decreases resolution, respectively. This can be avoided by using a second fluorescent dye as a reference for the incident light flux intensity, which is called Ratiometric or Two-Color Laser Induced Fluorescence (2C-LIF). The second dye normally shows a different temperature dependency or a temperature independency to extract the influence of the changing incident light flux. Furthermore, the fluorescence wavelengths of the two dyes need to differ to be able to separate the two signals. Rhodamine 110 meets these demands and is used as the second dye. Figure 3 shows the absorption and emission spectra of Rhodamine B and Rhodamine 110 for different wavelengths λ and the wavelength of the used 532 nm Nd:YAG laser. The absorption and emission spectra might shift with the special type of the dyes, with the solvent and with the temperature. Hence, this plot only gives a rough idea of how the spectra look like. However, as shown in Figure 3, the 532 nm Nd:YAG laser is well suited for the excitation of Rhodamine B, but the absorption for the Rhodamine 110 is very low at the laser's wavelength and hence, the emission intensity is expected to be low compared to the emission intensity of the Rhodamine B.
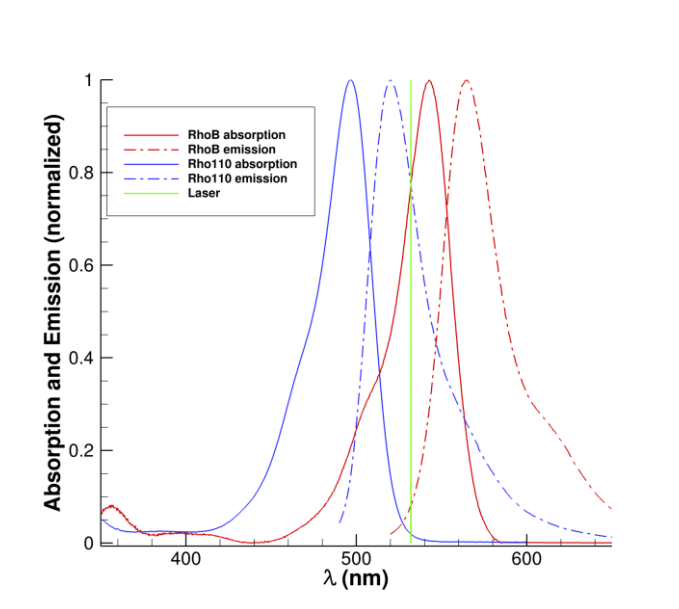
Figure 3: Absorption and emission spectra for Rhodamine B and Rhodamine 110, data partly obtained from [10, 11, 12].

3.1 Optical setup and analysis methods at the generic cooling duct

The velocity components in all three dimensions were measured with the use of 2C2D-PIV and 3C2D- PIV. The cameras were positioned to have a view on the xy plane and on the xz plane. An Nd:YAG double-pulse solid-state laser with a wavelength of 532 nm and an energy of 100 mJ per pulse is used for the illumination of the tracer particles and the excitation of the fluorescent dyes. The light sheet is focused by a plano-concave lens with a focal lenth of -50 mm and a plano-convex lens with a focal length of 100 mm. A cylindrical lens with a focal length of -25 mm forms the light sheet. The laser light sheet has a thickness of approximately 1 mm. PCO SensiCam cameras were used for the PIV and LIF measurements. The cameras have a low noise compared to other cameras and, for this reason, are particularly suitable for the LIF fluorescence signal. Tamron SP AF 180 mm lenses were used.

A spatial calibration was performed for all measurements in the generic cooling duct. For this purpose, a calibration grid was placed in the area of interest (AOI) in the test section. Images of the calibration grid at one position were used for 2C2D- and LIF-measurements, whereas two positions with an increment of 1 mm were used for 3C2D-measurements. The test section was filled with water during the calibration process to have identical optical distortions and refractions to the real measurements.

Silver-coated hollow glass spheres with a diameter of 10 µm were used for the PIV measurements. The 1C-LIF technique was applied in the generic cooling duct with Rhodamine B as the dye. A Rhodamine B concentration of 300 µg/l was used in this experiment. A bandpass filter with a center wavelength of 600 nm and a passing bandwidth of 20 nm was used. Double frame images were taken for PIV, whereas only single frame images with an exposure time of 80 ms after the laser pulse were acquired for LIF. A standard evaluation approach with a multipass technique with decreasing window size from 64 px × 64 px to 16 px × 16 px and 50% overlap was applied. All mean and turbulence plots are an average over x direction and are based on 1500 individual, statistically independent double frame images.

For the LIF, first, an average background image (image with closed camera lens) was subtracted from each individual image to eliminate for the camera's dark current. Second, the inhomogeneity of the laser light sheet and the transmission of the detection system were corrected at each individual image.

3.2 LIF characterization test setup and analysis methods

To improve and to gain experience about the 2C-LIF technique with Rhodamine B and Rhodamine 110, an additional test setup was designed for this purpose, see Figure 4. A container with three nontransparent walls and a lower side made of stainless steel was used with the front side made of a special glass with typical 99% transmittance and an anti-reflection coating. The cameras imaged the AOI, which was approximately in the middle of the container's depth. The laser light sheet entered the container from the top. The same laser with the same optical setup as described in the previous section was used. The laser light-sheet was oriented from the left hand side to the right hand side and was parallel to the AOI. A calibration grid was placed into the container parallel to the AOI and to the laser light sheet. The cameras were focused on that calibration grid. Hence, the laser light sheet was aligned with the cameras' focal point. Two cameras, PCO SensiCams, were used for recording the fluorescence signals. Different filters were used to get a good signal (strong fluorescence intensity) of each dye with respect to the emission spectra. Table 2 lists the used filters for separating each individual signal of the different dyes. One bandpass filter was used for recording only the Rhodamine B signal, and a second one for the Rhodamine 110 signal. To image a greater wavelength range of the emission spectra, longpass (LP) and shortpass (SP) edge filters were used: longpass filters to transmit the fluorescence signal of Rhodamine B, and shortpass filters to transmit the fluorescence signal of Rhodamine 110. The 532 nm laser light is in the range of the transmittance regime of the shortpass filters. Hence, a 532 nm notch filter was used additionally. The optical density of the edge filters is 4 and it is 6 for the notch filter. All filters have a diameter of 50 mm and were mounted between the camera and the lense. Lenses of the type Makro-Planar T 2/100 from Zeiss were used. The apertures of the lenses were "full open" to maximize brightness respectively fluorescence intensity. A cover encloses the whole setup and prevents reflecting light entering the camera. A sketch of the arrangement of the cameras, filters and lenses is given in Figure 5. The fluid was heated in the container using immersion heaters. The temperature was measured with a conventional bulk thermometer. With this setup, the fluid temperature was adjusted with an accuracy of approximately ±0.5 K. In the following, raw intensities are plotted without any data processing to get the real fluorescence intensities. An average of 10 individual images is used. The intensities are normalized with the maximum counts, which is 4095 for the used cameras. Chlorine free water was used as the solvent. The creation of a solution with an exact amount of dye is difficult because of the small amount of dye needed. Therefore, a solution with a larger amount / high concentration of Rhodamine was created. Then, all Rhodamine solutions were prepared for each individual series of measurement using parts of the solution with the high concentration. This method is quite exact; nevertheless a certain difference in intensity values is possible between two measurements due to this procedure.

Rhodamine B Filters (all values in nm)	Rhodamine 110 Filters (all values in nm)
BP 600 - 20	BP 550 - 20
LP 550	Notch 532 + SP 525
LP 575	Notch 532 + SP 550
LP 600	Notch 532 + SP 575

Table 2: Used filters.
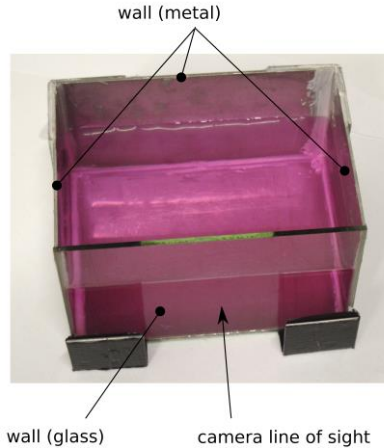
Figure 4: Container for fluorescence intensity measurements, filled with a Rhodamine B solution (600 µg/l).
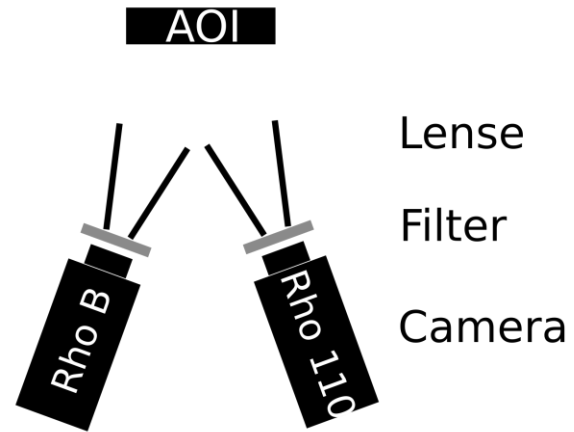

Figure 5: Arrangement of cameras, filters and lenses with respect to the Area Of Interest.

4   DUCT FLOW CHARACTERIZATION

The flow in the generic cooling duct is described in this section. First, the velocity field is described. Velocity profiles for the above described case 1 are given. Furthermore, a comparison of the velocity components and turbulent stresses for case1, case 2 and case 3 is given. The consistency and repeatability of the velocity data is not discussed in this paper. Please see Rochlitz et al. [13] for a detailed discussion of these topics. In addition to the measurements of the velocity field, basic measurements of the temperature fields in the generic cooling duct are given.

4.1   Velocity field

The mean flow in x direction is plotted in Figure 6 for three different $z/(w/2)$ positions. The velocity is large in the middle of the duct and is decreasing with decreasing absolute y/$(h/2)$ values and with increasing $z/(w/2)$ values. Hence, the velocity is high in the middle of the duct and is decreasing near the walls due to the no-slip condition. A plateau in the velocity profile is clearly visible in all plots at values of $z/(w/2) = 0.7$. This might be caused by strong secondary vortices which are present in this specific region. The velocity profile is nearly symmetrical with respect to the centerline at $z/(w/2) = 0$ for $z/(w/2) = 0$ and $z/(w/2) = 1/3$. The plot for $z/(w/2) = 2/3$ shows a non-symmetric behavior.

The y component of the velocity vector is plotted in Figure 7 for different $z/(w/2)$ positions. At the center line at $z/(w/2) = 0$, the fluid flows from the center of the duct to the upper and lower edge of the duct. An inflection point in the velocity is present at $y/(h/2) = \pm0.7$ values. This indicates the presence of vortex structures. The velocity profile near the outer wall shows an opposite behavior compared to the profile at the center line. All walls are masked for data evaluation. Because of that it is possible, that flow structures very near to the walls are not captured, which is the case in this plot. In comparison to the plot in Figure 11 inflection points very near the wall are missing in Figure 6 due to the mask. Hence, with the existence of one more inflection point near $y/(h/2) = \pm1$ values it can be stated that one additional weaker pair of vortex structures is present at $y/(h/2) = \pm0.92$ values.

Figure 8 depicts the velocity in x direction at discrete positions of $y/(h/2)$ over $z/(w/2)$. The velocity profiles agree to profiles already discussed. The small longitudinal velocity near the upper and lower is clearly visible. The velocity component in z direction is plotted in Figure 9. w/u_b is approximately zero in the core flow. At values near the upper and lower wall, the velocity component shows an s shaped behavior indicating the existence of secondary vortices.

All secondary vortices are in the order of 1 % of the bulk flow velocity which is in accordance with literature values.
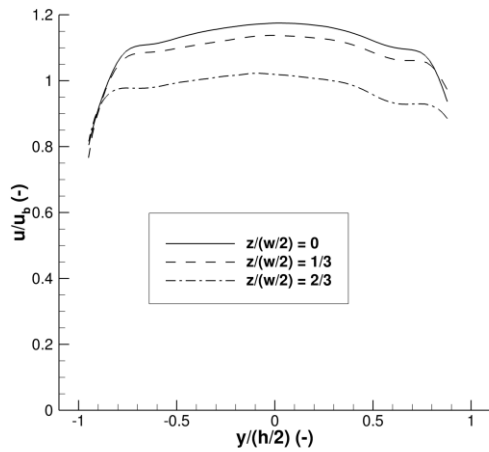
Figure 6: u/u_b at discrete z positions for case 1.
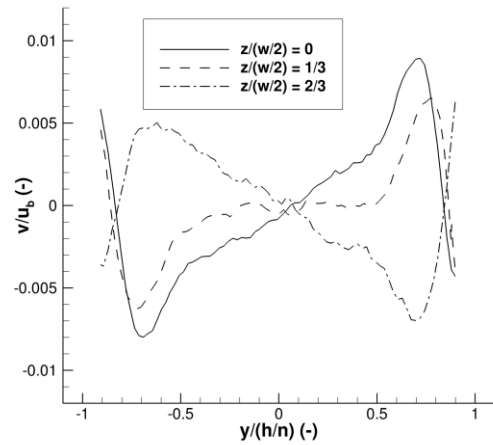
Figure 7: v/u_b at discrete z positions for case 1.
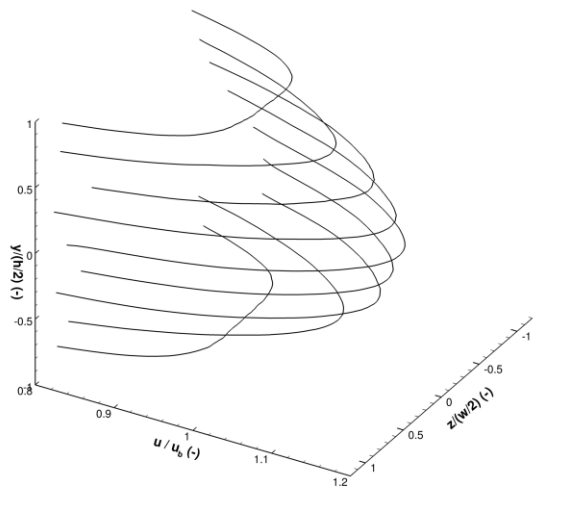
Figure 8: u/u_b at discrete positions of $y/(h/2)$ for case 1.
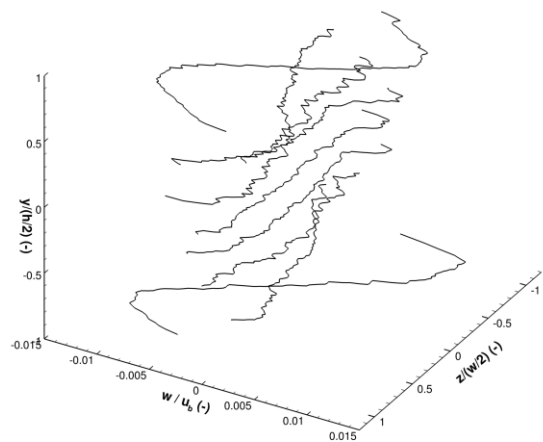
Figure 9: v/u_b at discrete positions of $y/(h/2)$ for case 1.

Figure 10 and Figure 11 display the mean longitudinal and vertical velocities for the different cases. Re doubles from case 1 to case 2 and the lower wall is heated in case 3 which leads to a significant heat flux. The longitudinal velocities are almost constant for all cases, whereas some minor changes in the vertical velocities exist. It seems that the secondary structures / vortex pairs as described above are increased slightly. Figure 12 to Figure 14 depict the turbulent stresses for the three different cases. The component $\overline{u'^2}/u_b^2$ changes with changing Re and with the applied heat flux. $\overline{v'^2}/u_b^2$ is affected by changing Re but not by the heated wall. The normalized shear stress $\overline{u'v'}/u_b^2$ remains constant for all three cases. In summary, it can be concluded that the flow is not very sensitive to a change in Re or to the application of a heat flux but some details show distinct sensitivities.
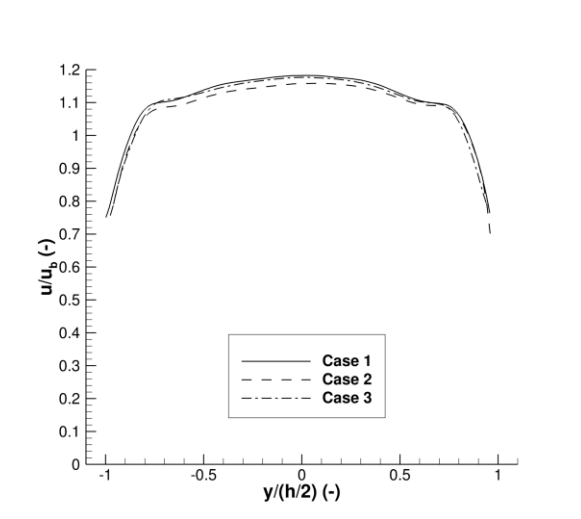
Figure 10: u/u_b case comparison.
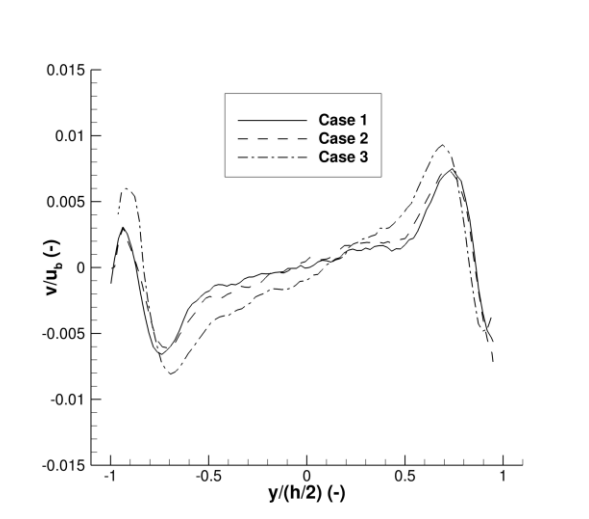
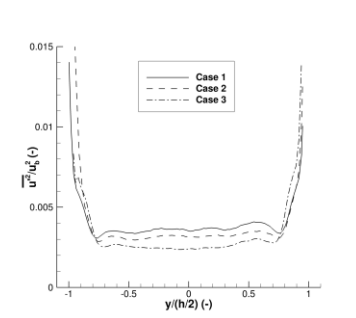Figure 11: v/u_b case comparison.

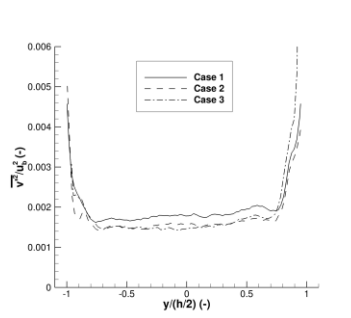Figure 12: $\overline{u'^2}/u_b^2$ case comparison.

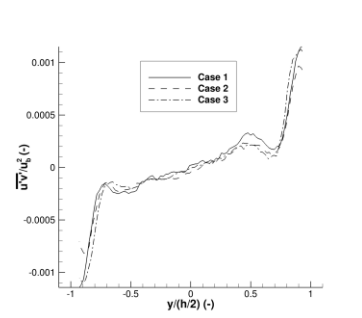Figure 13: $\overline{v'^2}/u_b^2$ case comparison.

Figure 14: $\overline{u'v'}/u_b^2$ case comparison.

4.2 Temperature field

An instantaneous temperature field with the thermal boundary layer in the generic cooling duct is pictured in Figure 15. A flow rate of 15 l/min, a bulk temperature of 20°C and a wall temperature of 75°C were set to get a better look at the thermal boundary layer. The flow direction is from the left to the right. The temperature field is given in intensity counts. The temperature near the wall is high and the temperature away from the wall at values around $y/(h/2) > -0.85$ values is constant and equal to the bulk temperature. Small hot plumes are visible, for example at $x/L \approx 0.01$. Figure 16 shows the mean temperature profile with a heated lower wall with a wall temperature of 100°C, a bulk temperature of approximately 47°C and a flow rate of 50 l/min. The temperature boundary layer is clearly and the uniform temperature in the bulk flow far away from the wall are clearly visible. The fluctuations in the region between $y/(h/2) > -0.7$ and $y/(h/2) > -0.2$ are due to o pollution on the cooling duct's walls. However, these results are not satisfying, since they do not allow for e.g. detailed analysis of temperature-velocity-fluctuations correlations. Therefore, a 2C-LIF technique shall be used. First general experimental results of these techniques are described in the next section.
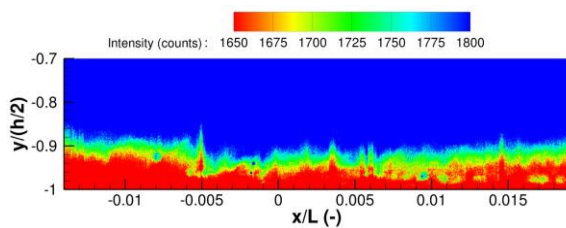

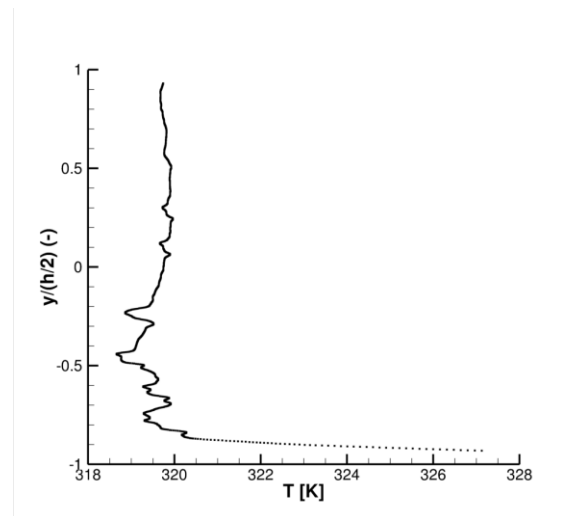Figure 15: Instantaneous temperature field.

Figure 16: Mean temperature profile with heated lower wall.

5   IMPROVEMENTS IN THE LIF TECHNIQUE

To obtain better results in the temperature fields in the generic cooling duct, improvements in the sensitivity of the LIF using different optical filters and different amounts of dyes are described in this section. Images of the fluorescences of the dyes are pictured in Figure 17 and Figure 18. These images were taken without any filters. High Rhodamine concentrations of 300 µg/l for Rhodamine B and 1500 µg/l for Rhodamine 110 were used in these cases to obtain images with very strong fluorescence intensities. The yellowish to orange fluorescence of the Rhodamine B is clearly visible and is easy to distinguish from the green laser light. The Rhodamine 110 fluorescence appears in a light green light and hence is not as easy to distinguish from the green laser light. However, the filters used for the intensity measurements are of high quality and do not transmit green laser light. Therefore, only the fluorescence is captured.

Figure 19 depicts the fluorescence intensities of Rhodamine B using different 'Rhodamine B filters (compare Table 2) over the Rhodamine B concentration. Normalized fluorescence intensity values of 1 means that

the camera sensor saturates. As expected, all fluorescence intensity values increase with increasing Rhodamine B concentrations and decrease with increasing temperature. All intensity values are well above the noise level which is at a value of 0.015. The BP600-20 filter which has been used in the past experiment shows the worst signal compared to the LP filters. The lower the edge wavelength of the LP is, the higher is the fluorescence signal, as one would generally expect, since a larger range of wavelengths can contribute to the signal This also allows for using a small amount of dye (Rhodamine B), for example 10 to 20 µg/L.

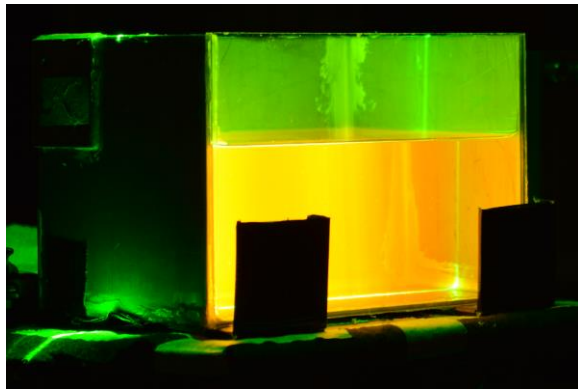Figure 17: Rhodamine B fluorescence at a concentration of 300 µg/l.

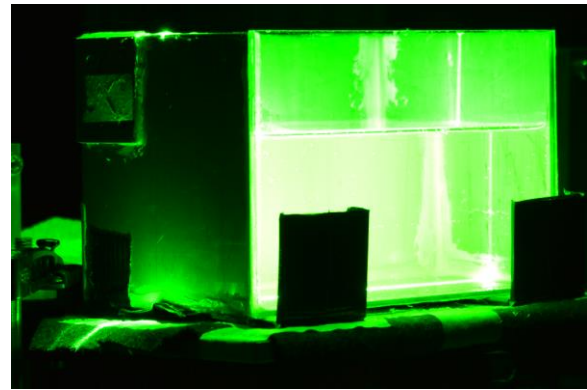Figure 18: Rhodamine 110 fluorescence at a concentration of 1500 µg/l.

The Rhodamine B fluorescence crosstalk to the Rhodamine 110 camera is plotted is Figure 20. The SP525 filter shows the lowest signal, followed by the SP550 filter. The BP550-20 filter shows a relatively high normalized signal of about 0.1, and the SP575 filter shows an even stronger signal of almost 1. Thus, both filters are not suitable for this application. Based hereon, SP525 or the SP550 filter should be used.

Figure 20 shows the Rhodamine 110 fluorescence signal crosstalk to the 'Rhodamine B camera. The Rhodamine 110 fluorescence intensity increases with temperature. This effect will be discussed later. The LP550 filter is at values larger 0.1 and hence not suitable. The value with the LP575 filter is about 0.04, which might be acceptable because the ratio to the Rhodamine B fluorescence signal is small. The LP600 and the BP600-20 show the smallest intensity values and hence, would, be suited best for the application. The fluorescence intensities of Rhodamine 110 with 'Rhodamine 110 filters' is plotted in Figure 21. The SP575 and the BP550-20 filters lead in the strongest intensity values, but are not suited for the application as already mentioned above. The SP550 and SP525 filters show weaker intensity values but the values are still a multiple of the noise when considering the values for 40°C. Hence, both filters are eligible. A concentration of about 600 µg/L should be used to get an adequate signal.

In summary, the LP600 filter and the LP575 filter are well suited for the application with the Rhodamine B camera in further applications. Concerning the Rhodamine 110 camera, the SP525 filter or the SP550 filter are a good choice.
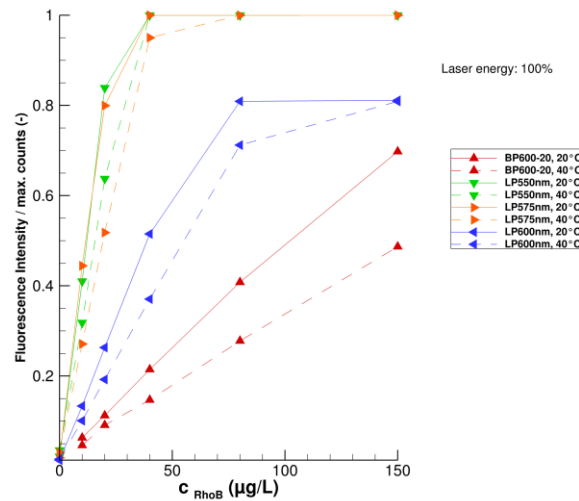
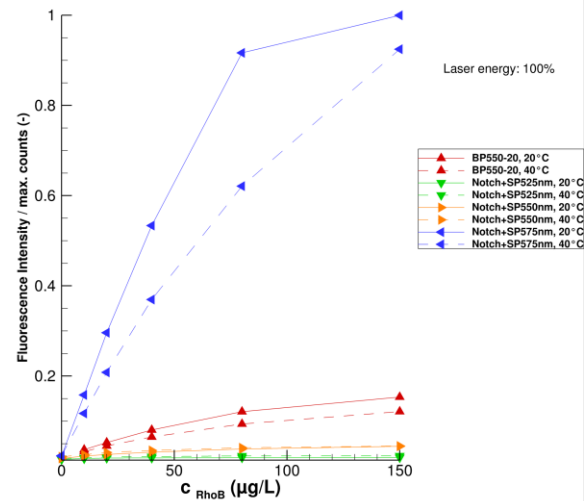Figure 19: Rhodamine B fluorescence intensities with different 'Rhodamine B filters'.

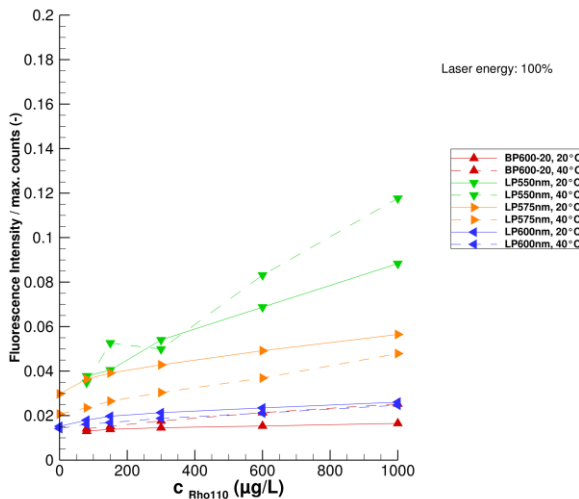Figure 20: Rhodamine B fluorescence intensities crosstalk to 'Rhodamine 110 camera.

Figure 21: Rhodamine 110 fluorescence intensities crosstalk to 'Rhodamine B camera.
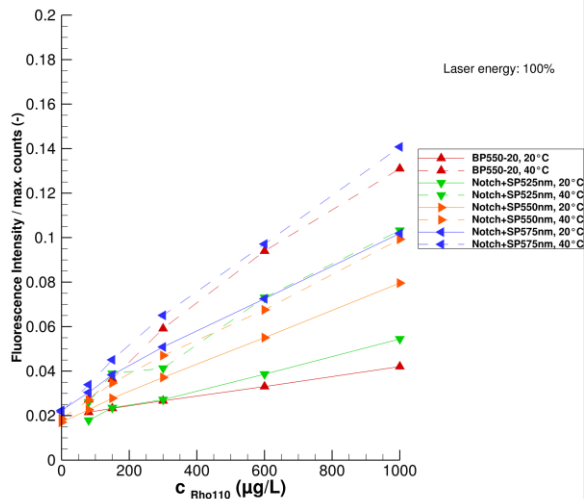

Figure 22: Rhodamine 110 fluorescence intensities with different 'Rhodamine 110 filters'.

The fluorescence intensity over laser energy is plotted in Figure 23 for different Rhodamine B and Rhodamine 110 concentrations with the LP600 filter for the Rhodamine B camera and the SP525 filter for the Rhodamine 110 camera. The fluorescence intensity significantly increases with increasing laser energy. The temperature dependence of both dyes is depicted in Figure 24. As expected, the Rhodamine B fluorescence intensity decreases with increasing temperature. The Rhodamine 110 fluorescence intensity increases with temperature. This is somewhat unexpected, because Rhodamine 110 fluorescence should be temperature independent. Most experiments, reporting a temperature independent fluorescence of Rhodamine 110 were conducted using Argon-Ion lasers at a wavelength of 488 nm [14, 15]. In contrast,

here the wavelength of 532nm of Nd:YAG laser is in a region of the Rhodamine 110 absorption spectrum, where the gradients are steep. We assume that the Rhodamine 110 absorption is not temperature independent -- the spectrum might shift with increasing temperature to larger wavelengths and hence, the absorption coefficient increases.

This is however not detrimental, because for the ratiometric analysis, using the ratio of the Rhodamine B and the Rhodamine 110 fluorescence intensities, this behavior of the Rhodamine 110 gives better temperature sensitivity.
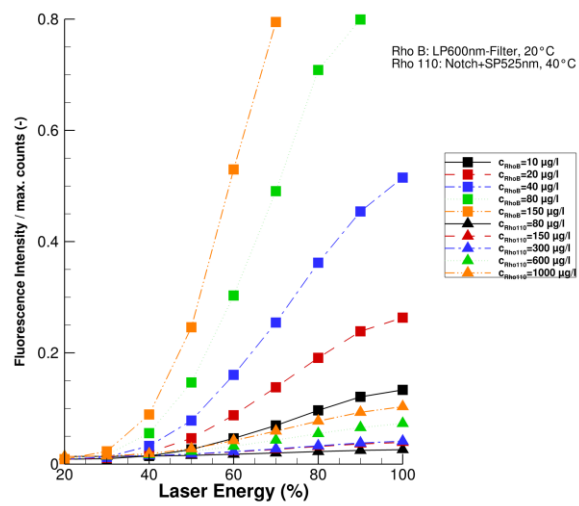

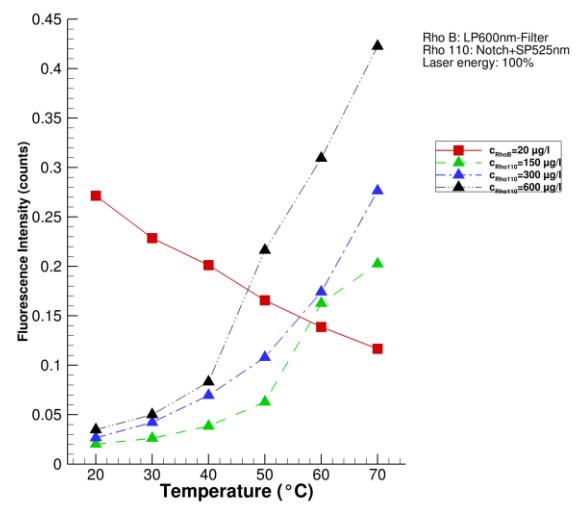Figure 23: Fluorescence intensities at different laser energy levels.

Figure 24: Fluorescence intensities at different temperatures.

6   SUMMARY

The flow in a rectangular, high aspect ratio cooling duct with one heated wall is characterized using the PIV and LIF measurement techniques using an Nd:YAG double pulse laser at a wavelength of 532nm. 2C2D-PIV and 3C2D-PIV are applied for quantifying the velocity fields at various positions in the xy plane and in the xz plane. Three cases with different parameters (changing Re, with and without wall heating) are considered. A detailed description of the flow field is given. One strong and one weak secondary vortex pair at each upper and lower side were identified in the v and w velocity profiles. The longitudinal velocity profile has a plateau at the position where the strong vortices are present. The velocity profiles do not show any significant change for all three cases. The Reynolds stresses are plotted: $\overline{u'^2}/u_b^2$ increases with increasing Re as well as with the application of the heat flux. $\overline{v'^2}/u_b^2$ and $\overline{u'v'}/u_b^2$ stay mostly constant for all cases.

The 1C-LIF technique is applied to the flow with the heated wall. The temperature field with the thermal boundary layer is plotted and heated strikes are visualized, however, sensitivity is not satisfying.

The 2C-LIF technique should be used in future experiments. An extensive study of fluorescence intensities with different filters at different temperatures and concentrations was conducted. A decrease in Rhodamine B fluorescence intensity and an increase in Rhodamine 110 fluorescence intensity was observed. It is recommend to use longpass filters with edge wavelengths of 575 nm or 600 nm for recording the signal of the Rhodamine B fluorescence and short pass filters with edge wavelength of 525 nm or 600 nm plus a

532 nm notch filter for recording the signal of the Rhodamine 110 fluorescence. The next step is the application of the 2C-LIF technique the generic cooling duct.

Acknowledgments

References

[1] Riccius, J., Haidn, O., Zametaev, E.: "Influence of Time Dependent Effects on the Estimated Life Time of Liquid Rocket Combustion Chamber Walls," 40th AIAA/ASME/SAE/ASEE Joint Propulsion Conference and Exhibit, pp. 1-12, 2004.

[2] Meyer, M. L.,: "Electrically Heated Tube Investigation of Cooling Channel Geometry Effects," NASA TM-106985, 1995.

[3] Meyer, M. L.,: "The effect of cooling passage aspect ratio on curvature heat transfer enhancement," NASA TN-107426, 1997.

[4] Sturgis, J. C., Mudawar, I.: "Single-phase heat transfer enhancement in a curved, rectangular channel subjected to concave heating," International Journal of Heat and Mass Transfer, Vol. 42, No. 7, 1999, pp. 12551272.

[5] Neuner, F., Preclik, D., Popp, M., Funke, M., Kluttig, H.: "Experimental and analytical investigation of local heat transfer in high aspect ratio cooling channels," AIAA-Paper 1998-3439-123, 1998.

[6] Wardana, I. N. G., Ueda, T., Mizomoto, M.:" Structure of turbulent two-dimensional channel flow with strongly heated wall," Experiments in Fluids, Vol. 13, No. 1, 1992, pp. 1725.

[7] Wardana, I. N. G., Ueda, T., Mizomoto, M.: "Effect of strong wall heating on turbulence statistics of a channel flow," Experiments in Fluids, Vol. 18, No. 1-2, 1994, pp. 87-94.

[8] Rochlitz, H., Scholz, P.: „Wärmeübergangs-Versuche an einer generischen Kühlkanalgeometrie", 63. Deutscher Luft- und Raumfahrtkongress, Augsburg, 15. September – 18. September 2014, DLRK 2014-340014

[9] Raffelel, M., Willert, C. E., Wereley, S. T., Kompenhans, J.: "Particle Image Velocimetry: A Practical Guide", 2nd ed., Springer Verlag, 1998.

[10] Life technologies: "Fluorescence SpectraViewer", http://www.lifetechnologies.com/de/de/home/ life-science/cell-analysis/labeling-chemistry/fluorescence-spectraviewer.html (2015/03/01)

[11] Du, H., Fuh, R. A., Li, J., Corkan, A., Lindsey, J. S.: "PhotochemCAD: A computer-aided design and research tool in photochemistry," Photochem. Photobiol., 68, 141-142, 1998.

[12] Dixon, J. M., Taniguchi, M., Lindsey J. S.: "PhotochemCAD 2. A refined program with accompanying spectral databases for photochemical calculations", Photochem. Photobiol., 81, 212-213, 2005.

[13] Rochlitz, H., Scholz, P.: "Application of Particle Image Velocimetry and Laser Induced Fluorescence in a cooling duct flow", 31st AIAA Aerodynamic Measurement Technology and Ground Testing Conference, June 22th – 26th, Dallas, USA

[14] Sakakibara, J., Adrian, R. J.:" Whole field measurement of temperature in water using two-color laser induced fluorescence", Experiments in Fluids, Vol.26, 1999, pp. 7-15

[15] Sakakibara, J., Adrian, R. J.:"Measurement of temperature field of a Rayleigh-Bénard convection using two-color laser-induced fluorescence", Experiments in Fluids, Vol. 37, 2004, pp. 331-340